Accepted Manuscript

One-pot synthesis of pH-responsive charge-switchable PEGylated nanoscale coordination polymers for improved cancer therapy

Yu Yang, Ligeng Xu, Wenjun Zhu, Liangzhu Feng, Jingjing Liu, Qian Chen, Ziliang Dong, Jiayue Zhao, Zhuang Liu, Meiwan Chen

PII: S0142-9612(17)30762-7

DOI: 10.1016/j.biomaterials.2017.11.038

Reference: JBMT 18376

To appear in: *Biomaterials*

Received Date: 13 November 2017

Accepted Date: 21 November 2017

Please cite this article as: Yang Y, Xu L, Zhu W, Feng L, Liu J, Chen Q, Dong Z, Zhao J, Liu Z, Chen M, One-pot synthesis of pH-responsive charge-switchable PEGylated nanoscale coordination polymers for improved cancer therapy, *Biomaterials* (2017), doi: 10.1016/j.biomaterials.2017.11.038.

One-pot synthesis of pH-responsive charge-switchable PEGylated nanoscale coordination polymers for improved cancer therapy

Yu Yang[1], Ligeng Xu[2], Wenjun Zhu[2], Liangzhu Feng[1], Jingjing Liu[2], Qian Chen[2], Ziliang Dong[2], Jiayue Zhao[2], Zhuang Liu[2]*, Meiwan Chen[1]*

1 State Key Laboratory of Quality Research in Chinese Medicine, Institute of Chinese Medical Sciences, University of Macau, Macau, China

2 Institute of Functional Nano & Soft Materials Laboratory (FUNSOM), Soochow University, Suzhou, Jiangsu 215123, China

Abstract: Nanoscale coordination polymers (NCPs) are promising nanomedicine platforms featured with biodegradability and versatile functionalities. However, multi-step post-synthesis surface modification is usually required to functionalize as-made NCPs before their biomedical applications. Moreover, efforts are still required to design therapeutic NCPs responsive to the unique tumor microenvironment to achieve more specific and effective therapy. Herein, we uncover a simple yet general strategy to synthesize a series of polyethylene glycol (PEG) modified NCPs via a one-step method by adding poly-histidine-PEG co-polymer into the mixture of metal ions and organic ligands during NCPs formation. With NCPs consisting Ca^{2+} / dicarboxylic cisplatin (IV) prodrug as the example, we show that such Ca/Pt(IV)@pHis-PEG NCPs are highly sensitive to pH changes. With slightly negative charges and compact structure under pH 7.4 during blood circulation, those NCPs exhibit efficient passive accumulation in the tumor, in which the reduced pH (c.a. 6.5) would trigger charge conversion and size expansion to enhance their tumor retention and cell internationalization. After cellular uptake, NCPs within cell endo-/lysosomes with further reduced pH would then lead to decomposition of those NCPs and thus drug release. Chemotherapy with Ca/Pt(IV)@pHis-PEG NCPs in our animal tumor model demonstrates great efficacy under low drug doses, and is found to be particularly effective towards solid tumors with reduced pH.

Key words: nanoscale coordination polymers (NCPs), one-pot synthesis, carrier-free drug delivery system, pH-responsive charge-switching, chemotherapy

Introduction:

The clinical outcomes of cancer chemotherapy drugs are limited by their off-target side effects and poor accumulation in solid tumors[1-3] Making use of the enhanced permeability and retention (EPR) effect, various kinds of nanoscale drug delivery systems (NDDSs), many of which with condensed polyethylene glycol (PEG) coating to realize 'stealth-like' long blood circulation behaviors, have been engineered to deliver anticancer agents into tumors via passive tumor targeting.[4-9] By conjugating targeting ligand recognizing tumor-specific receptors on the surface of nanoparticles, active tumor targeting has been proposed to further improve tumor targeting efficiency.[10] However, it is known that different types of tumors have varied levels of EPR effects, making the value of EPR-based passive tumor targeting arguable in clinical practices[11]. For ligand-receptor based active targeting, nanoparticles have to diffuse across the condensed extracellular matrix before recognizing tumor cells.[12, 13] The efficiency of this process may have considerable variations in different cases, not to mention large individual differences in tumor receptor expression levels[14]. Moreover, stealth nanoparticles trapped within the tumor may be gradually washed out by blood circulation, potentially reducing the long-term efficacy of nanomedicine.[15] Meanwhile, PEGylation of nanoparticles, although favorable for tumor-targeting, may hinder their cellular uptake and intercellular endosomal escape of drugs, limiting the anti-cancer efficacy of those drug-loaded nanoparticles.[16]

In recent years, accumulating clinical evidences have highlighted the crucial roles of the unique tumor microenvironment (TME) in tumor initiation and progression.[17-20] Notably, designing NDDSs responsive to the TME (e.g. reduced pH, hypoxia, specific types of enzymes) has emerged as an alternative strategy to improve tumor-targeting efficiency and specificity.[7, 21-29] Unlike in vivo tumor cell targeting for which the complex extra-cellular matrix is a barrier for NDDSs before tumor cell binding, targeting TME may be a more straightforward approach.[30, 31] Therefore, designing TME-responsive NDDSs has recently attracted tremendous attention.[22, 32-36] Despite a large number of encouraging results reported in this direction, many TME-responsive smart NDDSs have rather sophisticate designs[37-39]. Simple and robust methods to fabricate TME-responsive NDDSs are still needed to facilitate their clinical translation.

Nanoscale coordination polymers (NCPs) as well as metal-organic frameworks (MOFs) featured with structural/chemical diversities, highly enriched functionalities, well-defined

sizes/shapes, and intrinsic biodegradability have been widely explored in biomedicine, showing promises as multifunctional nano-platforms for carrying imaging agents, chemotherapeutics, gene therapeutics and photosensitizers.[40-51] Recently, in our group, we fabricated different types of nanoscale metal-organic frameworks (NMOFs) as biodegradable carrier-free systems for photothermal therapy and radiation therapy.[42, 43] Owing to the formation of NCPs based on non-covalent bonds, those metal organic structures could be decomposed in vivo, showing rapid renal clearance without long-term toxicity.[43] Notably, when NCPs are used for in vivo applications, their surface modification such as coating with polyethylene glycol (PEG) is an important step to improve the pharmacokinetics of those NCPs upon systemic administration so as to enable tumor targeting.[52, 53] However, in previously reported NCP-systems, surface PEGylation of NCPs usually involve multiple steps of reactions and modifications, and could be too complex for robust scaling-up production with high yields and efficiencies.[45, 54, 55] Moreover, the applications of NCPs or MOF-related nanostructures as smart anticancer nano-agents that are responsive to TME have not yet been reported to our best knowledge.

Hence, in this study, we develop a simple yet general strategy to synthesize a series of PEGylated NCP particles by an one-step reaction method. By mixing metal ions and organic ligands together with poly-L-histidine-PEG (pHis-PEG) co-polymer, in which the imidazole groups on the pHis chain could strongly bind with metal ions, PEGylated NCPs could be synthesized with high yields. Such a method is applicable for many metal ions such as Ca^{2+}, Tb^{3+}, Co^{2+}, Ni^{2+}, and Hf^{4+}, as well as various types of organic ligands including phosphorylated cisplatin prodrug, dicarboxylic cisplatin prodrug, and tris-(1-chloro-2-propyl) phosphate (TCPP). Subsequently, selecting NCPs consisting Ca^{2+} / dicarboxylic cisplatin (IV) prodrug as the example, we demonstrate that such Ca/Pt(IV)@pHis-PEG NCPs could act as a carrier-free pH-responsive nanomedicine drug for effective cancer therapy. Under pH 7.4, Ca/Pt(IV)@pHis-PEG nanoparticles with slightly negative surface charges and compact structure show prolonged blood circulation and efficient passive accumulation in the tumor. After entering TME with slightly acidic pH (e.g. 6.5), which would lead to the protonation of imidazole groups in pHis,[56, 57] the surface charge of Ca/Pt(IV)@pHis-PEG could be switched into positive and the nanoparticle sizes would be expanded, thereby enhancing tumor retention and cellular internalization of those nanoparticles. After cellular uptake, the further reduced pH inside endo-/lysosomes would trigger the decomposition of those NCPs and the

subsequent drug release for effective cancer cell killing. As evaluated in a mouse tumor model, our Ca/Pt(IV)@pHis-PEG is found to be a rather effective anti-tumor nanomedicine drug with excellent tumor suppression efficacy using relatively low drug doses upon systemic administration. Further mechanism study suggests that such tumor-targeted nanomedicine is indeed pH-responsive and works particularly well for tumors with acidic TME. Our work not only presents a general method for one-step synthesis of PEGylated NCPs, but also develops a unique TME-responsive nanomedicine drug promising for highly effective chemotherapy of cancer.

Materilas and methods

Materials:

Calcium chloride ($CaCl_2$) and hafnium chloride ($HfCl_4$) were obtained from Alfa Aesar. Cisplatin was bought from Beijing Zhongshuo Pharmaceutiful Technology Development Co., Ltd. Poly-(L-Histidine) (MW ~4500, ~33 amino acid residues) was purchased from GL Biochem (Shanghai) Ltd. Carboxylic acid functionalized polyethylene glycol (PEG-COOH, MW= 5K) was purchased from Biomatrik Inc. 3-(4,5-Dimethylthiazol-2-yl)-2,5-diphenyltetrazolium bromide (MTT), indocyanine green (ICG), Fluorescein (FITC), N-(3-Dimethylaminopropyl)-N-ethylcarbodiimide hydrochloride crystalline (EDC) and N-Hydroxysuccinimide (NHS) were obtained from Sigma-Aldrich. Other chemicals were obtained from Sinopharm Group Co. Ltd. All chemicals were used as received without further purification.

Synthesis of PEGylated NCPs:

Poly-(L-histidine)-PEG was prepared following a previous literature.[58] Firstly, 0.1mmol of poly-(L-histidine) was dissolved in DMSO as a stock solution. Next, 0.12 mmol of PEG-COOH was added into 20 mL of dichloromethane containing 0.12 mmol of EDC and 0.12 mmol of NHS under stirring for 2 h at room temperature. Subsequently, the stock solution was injected into the above mixture solution and stirred vigorously at room temperature for 2 days to finalize the reaction. After rotary evaporation, the product was dialyzed against distilled water for 2 days using a dialysis bag with the molecular weight cut-off (MWCO) of 3500 Da. Finally, the purified pHis-PEG was freeze-dried for future use.

For synthesis of c,c,t-$Pt(NH_3)_2Cl_2(OH)_2$, 0.5 g of cisplatin and 6.6 mL of H_2O_2 (30 wt%) was added in 2 mL of H_2O and then heated at 50 ^oC under vigorous magnetic stirring for 2 h in the dark and further stirred overnight at room temperature. Finally, the product was collected via vacuum filtration, washed with ethanol / diethyl ether, and vacuum dried. Pt (IV)-SA was synthesized by adding 3 mmol of c,c,t-$Pt(NH_3)_2Cl_2(OH)_2$ and 12 mmol of succinic anhydride into 3 mL of dimethyl sulfoxide (DMSO) and then reacted in the dark for 24 h at room temperature. After lyophilization, the product was precipitated by adding 20 mL of acetone and then dried after washing by acetone, diethyl ether three times.

For synthesis of bisphosphonic acid ligands based on Pt (IV) prodrugs, 3 mmol of c,c,t-$Pt(NH_3)_2Cl_2(OH)_2$ in dimethylformamide (DMF, 4 mL) was poured into a 1 mL of DMF solution containing 6.0 mmol of the diethoxyphosphinyl isocyanate, and then stirred in the dark for 12 h at room temperature. The product was obtained after precipitation by diethyl ether, filtration, and washing with diethyl ether. Next, after drying under vacuum for 10 h, 4 mL of dry DMF containing 0.36 mmol of bisphosphonate ester complex was added with 475 uL of trimethylsilyl bromide (TMSBr) and reacted in the dark at room temperature under nitrogen protection for 20 h. To hydrolyze the silyl ester, the product was dissolved in methanol and stirred at room temperature for 20 h after washing with DCM for at least twice.

To prepare Ca/Pt(IV)@pHis-PEG, Co/Pt(IV)@pHis-PEG, Ni/Pt(IV)@pHis-PEG, Hf/Pt(IV)@pHis-PEG and Tb/Pt(IV)@pHis-PEG NCPs, the respective metal chloride was firstly dissolved in 60 ml methanol containing 100 μL triethylamine (TEA). Then, 50 mg of pHis-PEG and 30 mg of Pt (IV)-SA pre-dissolved in 500 μL DMSO was added dropwisely. The reaction mixture was stirred for 24 h, collected by centrifugation and then washed with methanol for three times. After vacuum drying to remove the solvent, the final purified products were stored at 4 ^oC for future use. Ca/ phosphorylated Pt(IV)@pHis-PEG NCPs were prepared by the same method just by replacing Pt(IV)SA with phosphorylated Pt(IV). Ca@pHis-PEG nanoparticles were prepared by the same method just without adding phosphorylated Pt(IV). Fluorescently labeled Ca/Pt(IV)@pHis-PEG NCPs were prepared by adding 1 mg FITC or ICG into the mixture of pHis-PEG and Pt (IV)-SA in 500 μL DMSO during the synthesis process.

For synthesis of Hf/TCPP@pHis-PEG, $HfCl_4$ was dissolved in 60 mL of methanol solution containing 100 μL of TEA. Then, 50 mg of pHis-PEG and 30 mg of phosphorylated Pt(IV)

pre-dissolved in 500 μL DMSO was added dropwisely. The reaction mixture was stirred for 12 h, concentrated by rotary evaporator and then dialyzed against deionized water for 2 days within a dialysis bag (MWCO: 8-14 kDa). The final purified product was stored at 4 ^{o}C for future use.

Characterization of NCPs:

Transmission electron microscopy (TEM) imaging, elemental mapping and energy dispersive spectra (EDX) of those PEGylated NCPs were observed using a FEI Tecnai F20 transmission electron microscope at an acceleration voltage of 200 kV. The dynamic light scattering (DLS) and zeta potential measurements of those PEGylated NCPs were performed using a Zetasizer Nano-ZS (Malvern Instruments, UK). UV-Vis-NIR absorption spectra were recorded with a PerkinElmer UV-Vis spectrophotometer. To study the release kinetics of cis-Pt(IV) at pH 5.5, 6.5 and 7.4, we collected the released free cis-Pt(IV) in the supernatants after centrifugation at 14800 rpm for 10 min. Those collected solutions at different points were dissolved using aqua regia to measure Pt concentration by ICP-MS (Element 2, Thermo).

In vitro experiments:

Murine breast cancer 4T1 cells were obtained from American Type Culture Collection (ATCC) and cultured in standard cell culture medium with 10% fetal bovine serum (FBS) and 1% penicillin/streptomycin at 37 ^{o}C in a 5% CO_2-containing atmosphere. For cellular internalization of NCP-PEG, 4T1 cells were incubated with FITC-labeled NCP-PEG in DMEM medium at pH 6.5 or 7.4. Two hours later, the cells were washed twice with PBS and then observed using a laser scanning confocal microscope (LeciaSP5). Meanwhile, those cells were also analyzed using a BD Calibur flow cytometer. For *in vitro* cytotoxicity assay, 4T1 cells were seeded into 96 well plates and treated with different concentrations of free cisplatin, Ca/Pt(IV)@pHis-PEG or Ca-pHis-PEG for 48 h. After cells were washed with fresh cell culture medium, the standard MTT assay was carried out to measure the relative cell viabilities.

In vivo tumor model:

Balb/c mice were obtained from Nanjing Pengsheng Biological Technology Co. Ltd and used according to protocols approved by Sochoow University Laboratory Animal Center. To develop the

tumor model, Balb/c mice were subcutaneously injected with 2×10^6 4T1 cells within 50 μL of serum-free cell culture medium.

In vivo Imaging:

For *in vivo* fluorescence imaging, ICG-labeled Ca/Pt(IV)@pHis-PEG NCPs (ICG dose 1 mg/kg) was injected into tumor-bearing mice via the tail vein. At 1 h, 2 h, 4 h, 6 h, 8 h, and 24 h p.i., mice were anesthetized and imaged using the Maestro in vivo fluorescence imaging system. The auto-fluorescence was deducted by the spectrum unmixing software.

Blood circulation and biodistribution:

For blood circulation measured, mice were i.v. injected with ICG-labeled Ca/Pt(IV)@pHis-PEG NCPs. Blood was collected from each mouse at different time points and dissolved in a lysis buffer. The fluorescence intensity of each sample was measured using the Varioskan Flash Multiscan Spectrum. For analyzing the biodistribution profiles of NCPs, 4T1 tumor-bearing mice were i.v. injected with Ca/Pt(IV)@pHis-PEG. After 24 h, mice were sacrificed and the major organs were collected and dissolved using aqua regia to measure Pt concentrations by ICP-MS. For long-term biodistribution, after i.v. injection of Ca/Pt(IV)@pHis-PEG, tumor-free mice were scarified at 1 day and 7 days p.i. with their major organs collected and dissolved using aqua regia to measure Pt concentrations by ICP-MS.

For ICP-MS performance, blood samples, organs or tissues were collected, weighed, and solubilized in digesting solutions (VHNO3: VHCl: VHClO4= 3:1:2) by heating to boiling for 2 h. After cooling down to room temperature, each of resulting solutions was then diluted by DI water to 10 ml, and subsequently analyzed by ICP-MS to determine the total amount of Pt.

In vivo chemotherapy:

Balb/c mice bearing 4T1 tumors were randomly divided into four groups after the tumors reached ~ 70 mm^3 (n=5 for each group). Mice were treated by i.v. injected with PBS solution, free cisplatin (3 mg/kg), Ca-pHis-PEG, or Ca/Pt(IV)@pHis-PEG at the cisplatin dose of 3 mg/kg (for the second and fourth groups) for four times on day 0, day 2, day 4 and day 6. After different treatments, the tumor sizes and body weights were measured for individual animals every the other day. The

tumor size was calculated according to the following formula: tumor volume = (tumor length) × (tumor width)^2/2. Subsequently, relative tumor volumes were determined as V/V_0 (V_0 was the initiated volume). After various treatments, the tumor tissues were harvested to make paraffin section for further hexatoxylin and eosin (H&E) and terminal deoxynucleotidyl transferase-mediated dUTP-biotin nick end labeling (TUNEL) staining according to the manufacturer's protocols.

pH-dependent behaviors of NCPs inside the tumor

Photoacoustic pH imaging of tumor in mouse models was determined according to the previous report.[59] At 24 h post i.v. injection of HAS-Croc, photoacoustic imaging (PA) of mice was performed with photoacoustic computerized tomography scanner using VisualSonic Vevo 2100 LAZR system. To study how tumor pH would affect tumor uptake of NCPs, 4T1 tumor-bearing mice were i.t. injected with 20 μL of CAI (4-[[[(4-Fluorophenyl)amino]carbonyl]amino]-benzenesulfonamide (U-104), dose = 25 μM, Selleck, China). After 12 h, ICG-labeled Ca/Pt(IV)@pHis-PEG was i.v. injected into mice with or without CAI pre-treatment. After another 24 h, the mice were anesthetized and imaged using the Maestro in vivo fluorescence imaging system. Meanwhile, the tumors of mice were collected for ex vivo fluorescence imaging.

For flow cytometry analysis of tumors and confocal fluorescence imaging of tumor slices, mice with or without CAI pre-treatment were i.v. injected with FITC-labeled Ca/Pt(IV)@pHis-PEG and sacrificed at 24 h p.i. Tumors were collected and divided into two halves. To prepare flow cytometry samples, fresh tumor tissues were homogenized in lysis buffer to obtain the tumor cells. After incubation with red blood cell lysis buffer for 3 min, the tumor cells were centrifuged and then washed twice with PBS. The collected tumor cells were suspended in PBS with 1% fetal bovine serum (FBS) for flow cytometer measurement to determine the cellular uptake of FITC-labeled nanoparticles. The other halves of tumors were frozen-sectioned and then incubated with rat anti-CD31 mouse monoclonal antibody (Biolegend) and subsequently with Rhodamine-conjugated donkey anti-rat secondary antibody (Jackson) to stain the blood vessels. Fluorescence imaging of tumor slices was carried out by LeciaSP5 laser scanning confocal microscope.

Results and discussion:

Synthesis and characterization of PEGylated NCPs

The process for one-pot synthesis of PEGylated NCPs is illustrated in **Scheme 1**. In a typical experiment, dicarboxylic cisplatin(IV) prodrug as an organic linker and pHis-PEG as a stabilizing agent were dissolved in dimethyl sulfoxide (DMSO), and then slowly injected into 50 mL of methyl alcohol solution containing calcium chloride and triethylamine (TEA). After being stirred for additional 12 hours at room temperature, PEGylated NCPs, Ca/Pt(IV)@pHis-PEG nanoparticles were form with a high yield (~82 %). In this structure, owing to the binding of imidazole groups with Ca^{2+} ions, the pHis chain would be embedded within NCPs while the PEG chain in the pHis-PEG co-polymer would be extended outside to improve the water-solubility and physiological stability of those nanoparticles. As shown by transmission electron microscopy (TEM) **(Figure 1a**), Ca/Pt(IV)@pHis-PEG nanoparticles showed spherical morphology and narrow size distribution. The average hydrodynamic diameter of those NCPs was measured by dynamic light scattering (DLS) to be ~ 50 nm. To further illustrate the structures and confirm the compositions of as-synthesized NCPs, UV-Vis-NIR **(Supporting Figure S1)**, energy dispersive spectra (EDX) **(Supporting Figure S2)**, scanning TEM imaging with energy-dispersive X-ray spectroscopy (STEM-EDS) mapping**(Figure 1a, middle column)** and Powder X-ray diffraction (PXRD) patterns **(Supporting Figure S3)** were carried out. The even distribution of Ca and Pt elements in the obtained nanostructures further evidenced the successful formulation of NCPs. Similar to Ca/Pt(IV), Ca/Pt(IV)@pHis-PEG was also structurally amorphous yielding no peaks measured by PXRD. Meanwhile, revealed by BrunauereEmmetteTeller (BET) measurement, such amorphous NCPs exhibited quite large pore size at 10.2 nm and relatively high surface area at 67.45m^2/g **(Supporting Figure S4)**. We then extended our method to the synthesis of different NCP structures with varied organic ligands and metal ions. A series of PEGylated NCPs were successfully synthesized with dicarboxylic cisplatin(IV) prodrug, phosphorylated cisplatin(IV) prodrug or TCPP as organic linkers, and Ca^{2+}, Tb^{3+}, Co^{2+}, Ni^{2+}, or Hf^{4+} as metallic nodes, by adding poly-histidine-PEG co-polymer as a stabilizing agent during the formation of NCPs. As revealed by TEM imaging, EDX and DLS measurements, different types of PEGylated NCPs, including Tb/Pt(IV)@pHis-PEG, Co/Pt(IV)@pHis-PEG, Ni/Pt(IV)@pHis-PEG, Hf/Pt(IV)@pHis-PEG, Ca/phosphorylated Pt(IV)@pHis-PEG, and Hf/TCPP@pHis-PEG, have all been successfully synthesized with this method (**Figure 1b& Supporting Figure S5**), showing sizes ranging from ~20 nm to ~ 200 nm. Hence, a general one-step synthesis method is developed in our

work to prepare various types of PEGylated NCPs with narrow size distribution. Such a method is a rather simple straightforward one with high yields (over 80% for all different **NCPs** synthesized in this work).

Among various types of PEGylated NCPs synthesized above, Hf/TCPP@pHis-PEG NCPs containing photosensitizer TCPP may be used for photodynamic cancer therapy **(Supporting Figure S6)**[42, 60], while cis-Pt(IV) prodrug containing NCPs could be directly used for cancer chemotherapy. Considering that Ca^{2+} is a highly rich element in our body, we therefore chose Ca/Pt(IV)@pHis-PEG for following experiments to evaluate its ability in cancer treatment.

pH-dependent charge conversion and drug release profiles

Poly-histidine, a peptide containing imidazole groups with pI at 6.0, would show pH responsive charge conversion ability from neutral to positive due to protonation of imidazole within mild acidic environment.[57] We therefore carefully studied how our Ca/Pt(IV)@pHis-PEG NCPs would response to pH changes in solutions. We firstly measured zeta potentials of those NCPs under switched pHs between 7.4 and 6.5 **(Figure 2a)**. While being slightly negative under pH 7.4 with zeta potential at -2 mV, the surface charge of those NCPs containing pHis would be increased to be positive with zeta potential at 6~7 mV under pH 6.5. The hydrodynamic sizes of those nanoparticles were measured by DLS after incubation in phosphate buffered saline (PBS) with different pHs (7.4, 6.5, 5.5) over time **(Figure 2b)**. With persistent particle sizes at ~ 55 nm under pH 7.4 for 24 h **(Supporting Figure S8)**, our Ca/Pt(IV)@pHis-PEG nanoparticles showed gradually enlarged sizes under reduced pHs. After incubation for 60 min in those buffers, the DLS measured mean nanoparticle size increased to be ~130 nm under pH 6.5, and to be as large as over 700 nm under pH 5.5. To verify the size change of those NCPs, TEM imaging was then conducted to examine Ca/Pt(IV)@pHis-PEG samples after incubation with various buffers for 60 min **(Figure 2c)**. After exposure to slightly reduced pH at 6.5, obvious size expansion of NCPs was observed. Notably, incubation of those NCPs at further reduced pH (pH 5.5) would result in deformation of NCP structures and aggregation of nanoparticles, leading to greatly enlarged particle sizes under DLS measurement. Such a phenomenon could be explained by the protonation of imidazole groups to weaken the binding of pHis with Ca^{2+}, resulting in loosened NCP structure under pH 6.5 and complete deformation of this structure under further lowered pH at 5.5.

We next evaluated the pH-responsive drug release profiles of our Ca/Pt(IV)@pHis-PEG NCPs by incubating those nanoparticles in PBS with different pH values. The released cis-Pt(IV) was collected and dissolved using regia to measure Pt concentrations by inductively coupled plasma mass spectrometry (ICP-MS). As shown in **Figure 2d**, the time-dependent release of Pt from NCPs was found to be rather sensitive to pH. After incubation in PBS with pH values at 7.4 or 6.5 for 24 h, ~19% or ~37% of free cis-Pt(IV) was released from NCPs, respectively. In contrast, under further reduced pH at 5.5, over 95% of cis-Pt(IV) was released within the first 4 h. Such efficient acid-triggered drug release of Ca/Pt(IV)@pHis-PEG under pH 5.5 could be attributed to the decomposition of NCP structures under reduced pH, indicating the possible efficient drug release from NCPs inside acidic late endosomes and lysosomes after cellular uptake of those nanoparticles.[61]

pH-dependent intracellular internalization and in vitro cytotoxicity

Next, the in vitro cytotoxicity of NCP-PEG towards 4T1 cells was evaluated using 4T1 murine breast cancer cells. As the control, Ca-pHis-PEG, a nanoparticle system without drug loading (see method section for its preparation), showed high biocompatibility and little cytotoxicity towards 4T1 cells even at high concentrations after incubation for 48 hours **(Supporting Figure S7)**. In contrast, Ca/Pt(IV)@pHis-PEG showed obvious concentration-dependent cytotoxicity comparable to that of free cisplatin, indicating that cisplatin prodrug in such NCPs remained to be effective in killing cancer cells **(Figure 3a)**.

It is known that positively charged nanoparticles usually would exhibit enhanced cellular uptake owing to the stronger electrostatic interactions between those nanoparticles and cell membranes with negative surface charges. The cellular uptake efficiency of Ca/Pt(IV)@pHis-PEG and the in vitro therapeutic effects of these nanoparticles were then investigated under different pH values. Firstly, to facilitate the tracking of our NCPs, we doped a small amount of fluorescein isothiocyanate (FITC), a fluorescent dye, into NCPs by simply adding FITC during synthesis of Ca/Pt (IV)@pHis-PEG **(Supporting Figure S9)**. Murine breast cancer 4T1 cells were incubated with FITC-labeled Ca/Pt (IV)@pHis-PEG in standard cell culture medium (pH 7.4) or pH-adjusted acidic cell culture medium (pH= 6.5) for 2 h. As observed by confocal laser scanning microscopy (CLSM) **(Figure 3b),** NCP-treated cells cultured under pH 7.4 showed relative weak fluorescence inside cells, while those cultured in acidic cell culture medium at pH 6.5 displayed much stronger intracellular fluorescence,

indicating the significantly enhanced cellular uptake of NCPs induced by their surface charges conversion under the acidic condition. Quantitative flow cytometry **(Figure 3c)** measurement further revealed that the cellular uptake of those NCPs was enhanced by 5.2 times by switching the cell culture pH from 7.4 to 6.5.

Considering the significantly enhanced cellular uptake efficiency of NCPs under reduced pH, we then wondered whether the in vitro cancer cell killing efficiency of Ca/Pt(IV)@pHis-PEG would also be affected by pH values. In this experiment, 4T1 cells were incubated with Ca/Pt(IV)@pHis-PEG NCPs within cell culture at either pH 7.4 or pH 6.5 for 4 h, washed with PBS, and then cultured for another 20 h in drug-free cell culture medium (pH 7.4). As shown in **Figure 3d**, compared to cells incubated with Ca/Pt(IV)@pHis-PEG nanoparticles under pH 7.4, nanoparticle-incubated cells at pH 6.5 showed obviously lower cell viability, owing to enhanced intracellular internalization of NCPs under reduced pH. Our results thus collectively demonstrate that such Ca/Pt(IV)@pHis-PEG NCPs could act as a pH-responsive nanomedicine-drug with enhanced efficacy under acidic pH.

In vivo optical imaging, pharmacokinetic and biodistribution studies

Next, we carefully studied the in vivo behaviors of NCP-PEG in tumor-bearing mice. Firstly, the blood circulation of free cisplatin andCa/Pt(IV)@pHis-PEG was investigated by inductively coupled plasma mass spectrometry (ICP-MS, Element 2, Thermo) to determine the concentration of Pt in the blood samples collected at a series of time points post injection of these NCPs. As shown in figure 4a, free Pt(IV)showed quite fast blood clearance, while Ca/Pt(IV)@pHis-PEG in the blood was slowly cleared and remained at a relatively high concentration at 24 h post injection (p.i.). Furthermore, it was found that blood circulation of Ca/Pt(IV)@pHis-PEG followed a two-compartment model. The half-lives of the first and second phases of blood clearance were calculated to be 0.40 ± 0.21 h and 6.41 ± 0.52 h, respectively.

Next, indocyanine green (ICG), a clinically approved near-infrared (NIR) dye, was doped into Ca/Pt(IV)@pHis-PEG NCPs without leakage **(Supporting Figure S10&S11)** to track it's in vivo distribution in mice bearing 4T1 murine breast cancer tumors using in vivo fluorescence imaging **(Figure 4b)**. The fluorescence of ICG was observed throughout the whole mouse body at the early time points, whereas obvious tumor accumulation of Ca/Pt(IV)@pHis-PEG and high

tumor-to-normal contrast showed up later on. Major organs including liver, spleen, kidney, heart, lung and tumor were collected from mice 24 h after i.v. injection of ICG-labeled Ca/Pt(IV)@pHis-PEG for ex vivo fluorescence imaging **(Figure 4c)**. Strong ICG fluorescence from the tumor was detected. In addition, kidneys also showed strong fluorescence signals, indicating that these NCPs after their gradual decomposition inside the complicated in vivo environment might be effectively removed from the body via kidneys, consistent to our previously reported results.[43]

Post i.v. injection of Ca/Pt(IV)@pHis-PEG or free cisplatin, tumors and those major organs and tissues were collected and then dissolved using aqua regia for quantitative biodistribution measurement by ICP-MS to determine the concentrations of Pt in various organs. As shown in **Figure 4d**, Compared with free Pt(IV) only, the Ca/Pt(IV)@pHis-PEG NCPs accumulated in remarkably high concentration in the tumor, with the 9.8 percent-of-injected-dose-per-gram-tissue (%ID/g) at 24 h p.i. Meanwhile, High levels of Pt were also noted in kidneys, liver and spleen. While Pt accumulation in kidney may indicate rapid clearance of NCPs after gradual decomposition, liver and spleen are retuculoendohelial system (RES) responsible for clearance of foreign nanoparticles **(Figure 4d)**. To further study the in vivo excretion kinetics, tumor-free Balb/c mice after i.v. injection of Ca/Pt(IV)@pHis-PEG were sacrificed at 1 day and 7 days post injection (p.i.), with Pt concentrations in various organs analyzed using ICP-MS **(Figure 4e)**. Interestingly, the measured Pt levels in various organs of mice rapidly decreased to rather low levels within 7 days. All those results together indicate that our Ca/Pt(IV)@pHis-PEG NCPs may be gradually decomposed into small molecules in the complicated in vivo environment over time[42, 43] to allow efficient body clearance, which is particularly favorable to minimize the long-term toxicity concern of those nanoparticles.

In vivo cancer therapy

Afterwards, the in vivo anticancer therapeutic effect of Ca/Pt(IV)@pHis-PEG was evaluated using Balb/c mice bearing 4T1 tumors. In our experiments, 20 mice with initial tumor sizes at ~70 mm^3 were randomly divided into four groups (5 mice per group), and then i.v. injected with PBS, Ca@pHis-PEG, cisplatin, or NCP-PEG, at the cisplatin dose of 3 mg/kg at day 0, 2, 4, and 6 for four times. After receiving various treatments, the mice were closely monitored (**Supporting Figure S12**) and their tumor sizes were recorded by a caliper every the other day (**Figure 5a**). Compared to

cisplatin which only showed temporary growth inhibition effect in the early days, it was found that Ca/Pt(IV)@pHis-PEG treatment at the same drug dose could significantly inhibit the tumor growth. Photographs **(Figure 5b)** and weights **(Figure 5c)** of 4T1 tumors resected from scarified mice in each group 16 days after anti-cancer therapy further confirmed that the tumor growth rate could be significantly restrained by Ca/Pt(IV)@pHis-PEG treatment, which appeared to be remarkably better than conventional chemotherapy with cisplatin.

To further evaluate the therapeutic effects, terminal deoxynucleotidyl transferase dUTP nick end labeling (TUNEL) **(Figure 5e)** and Hemataoxulin and Eosin (H&E) staining **(Figure 5f)** of tumor slices in different groups were conducted on for tumors collected from mice sacrificed at the second day post the fourth injection. From H&E staining images, it was uncovered that tumor cells in Ca/Pt(IV)@pHis-PEG treated group suffered from the most severe damage, with the typical characteristics of cell and tissue damages. In contrast, tumor cells in other three groups showed partly or largely maintained normal membrane morphology and nuclear structures. TUNEL staining results further illustrated that Ca/Pt(IV)@pHis-PEG treatment induced the highest level of tumor cells apoptosis among all different groups.

During such treatment, no appreciable body weight loss **(Figure 5d)** or noticeable sign of abnormal animal behaviors was noticed over 16 days for mice after treatment with Ca/Pt(IV)@pHis-PEG, indicating the absence of obvious acute toxicity of those NCPs to the treated mice. To further investigate the potential toxicity of our Ca/Pt(IV)@pHis-PEG NCPs, we then carefully performed histology examination for healthy Balb/c mice after i.v. injected with Ca/Pt(IV)@pHis-PEG (3 mg/kg of cis-Pt for each dose, 4 repeated doses). Major organs (liver, spleen, kidney, heart and lung) were collected and sliced for H&E staining (**Supporting Figure S13**). No obvious sign of organ damage or inflammatory lesion was observed for mice 30 days after i.v. injection of Ca/Pt(IV)@pHis-PEG, suggesting these NCPs would be a relatively safe agent without inducing significant long-term toxicity to the treated mice at our injected dose.

In vivo mechanism study of pH-dependent cancer treatment

It known that insufficient blood perfusion, hypoxia, and glycolytic cancer cell metabolism, which are common characteristics of solid tumors, could lead to the acidic TME with pH in the range of 6.0~7.0[62, 63]. Therefore, we hypothesized that such remarkably enhanced therapeutic effect

of Ca/Pt(IV)@pHis-PEG could be attributed to the acidic-responsive charge conversion and size expansion of those NCPs under the reduce TME pH (e.g. pH 6.5) in the tumor. Such a transformation may enhance the tumor retention and cell internationalization of those drug-loaded nanoparticles, so as to be favorable for nanomedicine treatment of solid tumors with reduced pH. To demonstrate this hypothesis, tumors on the mice were treated with carbonic anhydrase inhibitor (CAI), which could inhibit carbonic anhydrase activity in tumor cells to increase the TME pH inside tumors.[64] Careful experiments were then designed and carried out to understand how the tumor pH would affect the behaviors of our Ca/Pt(IV)@pHis-PEG nanoparticles inside tumors **(Figure 6a)**.

Firstly, we used our previously reported pH-sensitive albumin-based photoacoustic (PA) imaging probe, human serum albumin-croconine (HSA-Croc) nanoparticles, to detect the pH changes in the tumor by dual-wavelength ratiometric photoacoustic (PA) imaging.[59] Owing to the pH-responsive absorbance spectrum of HSA-Croc **(Supporting Figure S14)**, the photoacoustic signal ratio between 680 nm and 810 nm of HSA-Croc could be utilized to determine pH changes. 4T1-tumor-bearing mice were thus intravenously pre-injected with HSA-croc 24 h prior to PA imaging, which was conducted before and right after intra-tumor (i.t.) injection of citrate buffer (pH 5.5) or $NaHCO_3$ solution (pH 8.4) (**Figure 6b**). The 680:810 PA signal ratio showed instant drop as the decrease of tumor pH after injection of citrate buffer, and increased significantly as the rise of tumor pH post i.t. injection of $NaHCO_3$ solution **(Figure 6c)**, demonstrating the capability of ratiometric PA imaging with HSA-croc for in vivo pH detection. Thereafter, we tested the ability of CAI to weaken the tumor acidity. 24 h after i.t. injection of CAI (20 μL, 25 μM), mice pre-injected with HSA-croc nanoprobe were imaged under the PA scanner for tumor pH detection **(Figure 6b)**. Based on changes of 680/810 PA signal ratios, it was obviously that i.t. injection of CAI could induce significant increase of TME pH inside the tumor **(Figure 6c)**. Such en effect was similar to the injection of $NaHCO_3$ solution but could last for much longer (~ 1 week). Our results confirmed that CAI treatment could indeed result in significant increase of tumor pH.

Next, we evaluated whether our pH-responsive charge-switchable Ca/Pt(IV)@pHis-PEG nanoparticles would behave differently in the same tumor model but with different tumor pH. Balb/c mice bearing 4T1 tumors were i.t. injected with CAI (20 μL, 25 μM) to increase the tumor pH. One day later, mice were i.v. injected with ICG-labeled Ca/Pt(IV)@pHis-PEG NCPs and imaged by a Maestro EX in vivo imaging system **(Figure 6d)**. Compared to tumors without CAI pre-treatment,

tumors with increased pH after CAI treatment showed obviously reduced uptake of ICG-labeled Ca/Pt(IV)@pHis-PEG. Such a difference was further confirmed by ex vivo imaging of dissected tumors from mice 24 h post i.v. injection of nanoparticles **(Figure 6e)**. Therefore, the acidic tumor pH indeed contributed to the enhanced tumor retention of our pH responsive NCPs.

To further understand the behaviors of those NCPs within the tumor, 4T1-tumor-bearing mice with or without CAI treatment were i.v. injected with FITC-labeled Ca/Pt(IV)@pHis-PEG NCPs and sacrificed at 24 h post injection (p.i.). The dissected tumors were separated into two halves for both flow cytometry measurement and confocal fluorescence imaging. After tumor sections were homogenized and tumor cells were harvested, flow cytometry analysis was conducted to study the cellular uptake of FITC-labeled nanoparticles inside tumors (**Figure 6f**). Compared with tumor cells from mice treated with CAI, those collected from mice without CAI-treatment showed a much higher level of FITC signals, suggesting enhanced cell internalization of NCPs in tumors with acidic pH. Furthermore, tumor slices were extracted from the two group of mice and then stained with anti-CD31 antibody (red) to visualize blood vessels **(Figure 6g)**. Consistent to all previous results, CAI treatment to increase tumor pH would lead to significantly reduced tumor retention of FITC-labeled Ca/Pt(IV)@pHis-PEG NCPs **(Figure 6h)**. Our results collectively demonstrate that our Ca/Pt(IV)@pHis-PEG is a pH-responsive nanomedicine with greatly enhanced tumor retention and tumor cell internalization under reduced pH, particularly suitable for treatment of solid tumors with low TME pH.

Conclusion:

In summary, we have developed a simple and general strategy for one-step synthesis of a series of pH-responsive charge-switchable PEGylated NCPs, via adding pHis-PEG copolymer as a stabilizing agent and functional molecule into the mixture of metal ions and organic ligands during the formation process of NCPs. It is uncovered that Ca/Pt(IV)@pHis-PEG, a representative type of PEGylated NCPs fabricated in this work, appears to be highly pH-sensitive. While being stable with compact PEGylation and slight negative charges under pH 7.4, such Ca/Pt(IV)@pHis-PEG would convert into positive charged nanoparticles with expanded sizes under pH 6.5 (the TME pH), and then decomposed to release cis-Pt(IV) prodrug under further reduced pH at 5.5 (the lysosome pH after cellular uptake of nanoparticles). Such pH-responsive NCPs are found to be a highly effective

chemotherapy drug with remarkably improved in vivo therapeutic efficacy compared to free cisplatin. Carefully designed mechanism study further verify that our Ca/Pt(IV)@pHis-PEG NCPs indeed show pH-dependent behaviors inside the tumor. Our work therefore presents a novel type of therapeutic NCPs, which not only are composed by biocompatible safe components with inherent biodegradability, but also show pH-responsive tumor retention / tumor cell uptake behaviors to enable enhanced nanomedicine-based chemotherapy, which may be particularly effective for tumors with reduced pH. Furthermore, it is believed other types of PEGylated NCPs with pH-responsive behaviors prepared by the same one-step method may also find promising applications in nanomedicine.

Acknowledgments

This work was partially supported by the National Research Programs from Ministry of Science and Technology (MOST) of China (2016YFA0201200), the National Natural Science Foundation of China (51525203, 81403120), Collaborative Innovation Center of Suzhou Nano Science and Technology, and a Project Funded by the Priority Academic Program Development (PAPD) of Jiangsu Higher Education Institutions., the Macao Science and Technology Development Fund (096/2015/A3) and the Research Fund of the University of Macau (MYRG2016-00130-ICMS-QRCM).

Reference

[1] Peer D, Karp JM, Hong S, Farokhzad OC, Margalit R, Langer R. Nanocarriers as an emerging platform for cancer therapy. Nature nanotechnology. 2007;2:751-60.

[2] Danhier F, Feron O, Préat V. To exploit the tumor microenvironment: passive and active tumor targeting of nanocarriers for anti-cancer drug delivery. J Control Release. 2010;148:135-46.

[3] Misra R, Acharya S, Sahoo SK. Cancer nanotechnology: application of nanotechnology in cancer therapy. Drug Discov Today. 2010;15:842-50.

[4] Maeda H, Wu J, Sawa T, Matsumura Y, Hori K. Tumor vascular permeability and the EPR effect in macromolecular therapeutics: a review. J Control Release. 2000;65:271-84.

[5] Fang J, Nakamura H, Maeda H. The EPR effect: unique features of tumor blood vessels for drug delivery, factors involved, and limitations and augmentation of the effect. Advanced drug delivery reviews. 2011;63:136-51.

[6] Cheng Z, Al Zaki A, Hui JZ, Muzykantov VR, Tsourkas A. Multifunctional nanoparticles: cost versus benefit of adding targeting and imaging capabilities. Science. 2012;338:903-10.

[7] Chauhan VP, Stylianopoulos T, Martin JD, Popović Z, Chen O, Kamoun WS, et al. Normalization of tumour blood vessels improves the delivery of nanomedicines in a size-dependent manner. Nature nanotechnology. 2012;7:383-8.

[8] Yang Y, Wang S, Wang Y, Wang X, Wang Q, Chen M. Advances in self-assembled chitosan nanomaterials for drug

delivery. Biotechnol Adv. 2014;32:1301-16.

[9] Klibanov AL, Maruyama K, Torchilin VP, Huang L. Amphipathic polyethyleneglycols effectively prolong the circulation time of liposomes. FEBS letters. 1990;268:235-7.

[10] Nie S. Understanding and overcoming major barriers in cancer nanomedicine. Nanomedicine. 2010;5:523-8.

[11] Wilhelm S, Tavares AJ, Dai Q, Ohta S, Audet J, Dvorak HF, et al. Analysis of nanoparticle delivery to tumours. Nature Reviews Materials. 2016;1:16014.

[12] Li H-J, Du J-Z, Du X-J, Xu C-F, Sun C-Y, Wang H-X, et al. Stimuli-responsive clustered nanoparticles for improved tumor penetration and therapeutic efficacy. Proceedings of the National Academy of Sciences. 2016;113:4164-9.

[13] Qiu L, Chen T, Öçsoy I, Yasun E, Wu C, Zhu G, et al. A Cell-Targeted, Size-Photocontrollable, Nuclear-Uptake Nanodrug Delivery System for Drug-Resistant Cancer Therapy. Nano Letters. 2015;15:457-63.

[14] DiLillo David J, Ravetch Jeffrey V. Differential Fc-Receptor Engagement Drives an Anti-tumor Vaccinal Effect. Cell. 2015;161:1035-45.

[15] Amoozgar Z, Yeo Y. Recent advances in stealth coating of nanoparticle drug delivery systems. Wiley Interdisciplinary Reviews: Nanomedicine and Nanobiotechnology. 2012;4:219-33.

[16] Li S-D, Huang L. Stealth nanoparticles: high density but sheddable PEG is a key for tumor targeting. Journal of controlled release: official journal of the Controlled Release Society. 2010;145:178.

[17] Astarita JL, Cremasco V, Fu J, Darnell MC, Peck JR, Nieves-Bonilla JM, et al. The CLEC-2-podoplanin axis controls the contractility of fibroblastic reticular cells and lymph node microarchitecture. Nat Immunol. 2015;16:75-84.

[18] Quail DF, Joyce JA. Microenvironmental regulation of tumor progression and metastasis. Nat Med. 2013;19:1423-37.

[19] Bhowmick NA, Neilson EG, Moses HL. Stromal fibroblasts in cancer initiation and progression. Nature. 2004;432:332-7.

[20] Bissell MJ, Hines WC. Why don't we get more cancer? A proposed role of the microenvironment in restraining cancer progression. Nature medicine. 2011;17:320-9.

[21] Wang S, Huang P, Chen X. Hierarchical Targeting Strategy for Enhanced Tumor Tissue Accumulation/Retention and Cellular Internalization. Adv Mater. 2016.

[22] Sun Q, Sun X, Ma X, Zhou Z, Jin E, Zhang B, et al. Integration of nanoassembly functions for an effective delivery cascade for cancer drugs. Advanced Materials. 2014;26:7615-21.

[23] Chauhan VP, Jain RK. Strategies for advancing cancer nanomedicine. Nature materials. 2013;12:958-62.

[24] Yang Y, Wang SP, Wang YT, Wang XH, Wang Q, Chen MW. Advances in self-assembled chitosan nanomaterials for drug delivery. Biotechnology Advances. 2014;32:1301-16.

[25] Sun C-Y, Shen S, Xu C-F, Li H-J, Liu Y, Cao Z-T, et al. Tumor acidity-sensitive polymeric vector for active targeted siRNA delivery. Journal of the American Chemical Society. 2015;137:15217-24.

[26] Du J-Z, Du X-J, Mao C-Q, Wang J. Tailor-made dual pH-sensitive polymer–doxorubicin nanoparticles for efficient anticancer drug delivery. Journal of the American Chemical Society. 2011;133:17560-3.

[27] Yin Q, Tang L, Cai K, Tong R, Sternberg R, Yang X, et al. Pamidronate functionalized nanoconjugates for targeted therapy of focal skeletal malignant osteolysis. Proceedings of the National Academy of Sciences. 2016:201603316.

[28] Wang H, Gauthier M, Kelly JR, Miller RJ, Xu M, O'Brien WD, et al. Targeted Ultrasound‐Assisted Cancer‐Selective Chemical Labeling and Subsequent Cancer Imaging using Click Chemistry. Angewandte Chemie. 2016;128:5542-6.

[29] Park S, Kim E, Kim WY, Kang C, Kim JS. Biotin-guided anticancer drug delivery with acidity-triggered drug release. Chemical Communications. 2015;51:9343-5.

[30] Wang JQ, Mao WW, Lock LL, Tang JB, Sui MH, Sun WL, et al. The Role of Micelle Size in Tumor Accumulation, Penetration, and Treatment. Acs Nano. 2015;9:7195-206.

[31] Yang Y, Liu JJ, Sun XQ, Feng LZ, Zhu WW, Liu Z, et al. Near-infrared light-activated cancer cell targeting and drug

delivery with aptamer-modified nanostructures. Nano Res. 2016;9:139-48.
[32] Ernsting MJ, Murakami M, Roy A, Li S-D. Factors controlling the pharmacokinetics, biodistribution and intratumoral penetration of nanoparticles. J Control Release. 2013;172:782-94.
[33] Gratton SE, Ropp PA, Pohlhaus PD, Luft JC, Madden VJ, Napier ME, et al. The effect of particle design on cellular internalization pathways. Proceedings of the National Academy of Sciences. 2008;105:11613-8.
[34] Chen Q, Feng L, Liu J, Zhu W, Dong Z, Wu Y, et al. Intelligent Albumin–MnO2 Nanoparticles as pH-/H2O2-Responsive Dissociable Nanocarriers to Modulate Tumor Hypoxia for Effective Combination Therapy. Adv Mater. 2016.
[35] Miao L, Lin CM, Huang L. Stromal barriers and strategies for the delivery of nanomedicine to desmoplastic tumors. J Control Release. 2015;219:192-204.
[36] Han A, Wang H, Kwok RT, Ji S, Li J, Kong D, et al. Peptide-Induced AIEgen Self-Assembly: A New Strategy to Realize Highly Sensitive Fluorescent Light-Up Probes. Analytical chemistry. 2016;88:3872-8.
[37] Thomas CR, Ferris DP, Lee J-H, Choi E, Cho MH, Kim ES, et al. Noninvasive Remote-Controlled Release of Drug Molecules in Vitro Using Magnetic Actuation of Mechanized Nanoparticles. J Am Chem Soc. 2010;132:10623-5.
[38] Yavuz MS, Cheng YY, Chen JY, Cobley CM, Zhang Q, Rycenga M, et al. Gold nanocages covered by smart polymers for controlled release with near-infrared light. Nature Materials. 2009;8:935-9.
[39] Allen TM, Cullis PR. Drug delivery systems: Entering the mainstream. Science. 2004;303:1818-22.
[40] James SL. Metal-organic frameworks. Chem Soc Rev. 2003;32:276-88.
[41] Li Z-Q, Qiu L-G, Xu T, Wu Y, Wang W, Wu Z-Y, et al. Ultrasonic synthesis of the microporous metal–organic framework Cu 3 (BTC) 2 at ambient temperature and pressure: an efficient and environmentally friendly method. Materials Letters. 2009;63:78-80.
[42] Liu J, Yang Y, Zhu W, Yi X, Dong Z, Xu X, et al. Nanoscale metal– organic frameworks for combined photodynamic & radiation therapy in cancer treatment. Biomaterials. 2016;97:1-9.
[43] Yang Y, Liu J, Liang C, Feng L, Fu T, Dong Z, et al. Nanoscale metal–organic particles with rapid clearance for magnetic resonance imaging-guided photothermal therapy. ACS nano. 2016;10:2774-81.
[44] Liu D, Poon C, Lu K, He C, Lin W. Self-assembled nanoscale coordination polymers with trigger release properties for effective anticancer therapy. Nature communications. 2014;5.
[45] He C, Poon C, Chan C, Yamada SD, Lin W. Nanoscale Coordination Polymers Codeliver Chemotherapeutics and siRNAs to Eradicate Tumors of Cisplatin-Resistant Ovarian Cancer. J Am Chem Soc. 2016;138:6010-9.
[46] Diring S, Wang DO, Kim C, Kondo M, Chen Y, Kitagawa S, et al. Localized cell stimulation by nitric oxide using a photoactive porous coordination polymer platform. Nature Communications. 2013;4.
[47] Horcajada P, Gref R, Baati T, Allan PK, Maurin G, Couvreur P, et al. Metal-Organic Frameworks in Biomedicine. Chemical Reviews. 2012;112:1232-68.
[48] Zhou HC, Long JR, Yaghi OM. Introduction to Metal-Organic Frameworks. Chem Rev. 2012;112:673-4.
[49] Keskin S, Kızılel S. Biomedical applications of metal organic frameworks. Industrial & Engineering Chemistry Research. 2011;50:1799-812.
[50] Horcajada P, Gref R, Baati T, Allan PK, Maurin G, Couvreur P, et al. Metal–organic frameworks in biomedicine. Chemical reviews. 2011;112:1232-68.
[51] Horcajada P, Chalati T, Serre C, Gillet B, Sebrie C, Baati T, et al. Porous metal-organic-framework nanoscale carriers as a potential platform for drug delivery and imaging. Nature materials. 2010;9:172.
[52] He CB, Liu DM, Lin WB. Self-Assembled Core-Shell Nanoparticles for Combined Chemotherapy and Photodynamic Therapy of Resistant Head and Neck Cancers. Acs Nano. 2015;9:991-1003.
[53] Suk JS, Xu Q, Kim N, Hanes J, Ensign LM. PEGylation as a strategy for improving nanoparticle-based drug and gene delivery. Adv Drug Deliver Rev. 2016;99:28-51.
[54] Cohen SM. Modifying MOFs: new chemistry, new materials. Chemical Science. 2010;1:32-6.

[55] Wang ZQ, Cohen SM. Postsynthetic modification of metal-organic frameworks. Chem Soc Rev. 2009;38:1315-29.
[56] Lee ES, Na K, Bae YH. Polymeric micelle for tumor pH and folate-mediated targeting. J Control Release. 2003;91:103-13.
[57] Radovic-Moreno AF, Lu TK, Puscasu VA, Yoon CJ, Langer R, Farokhzad OC. Surface charge-switching polymeric nanoparticles for bacterial cell wall-targeted delivery of antibiotics. ACS nano. 2012;6:4279-87.
[58] Wang S, Yang Y, Wang Y, Chen M. Gambogic acid-loaded pH-sensitive mixed micelles for overcoming breast cancer resistance. International journal of pharmaceutics. 2015;495:840-8.
[59] Chen Q, Liu X, Zeng J, Cheng Z, Liu Z. Albumin-NIR dye self-assembled nanoparticles for photoacoustic pH imaging and pH-responsive photothermal therapy effective for large tumors. Biomaterials. 2016;98:23-30.
[60] Park J, Jiang Q, Feng D, Zhou H-C. Controlled Generation of Singlet Oxygen in Living Cells with Tunable Ratios of the Photochromic Switch in Metal–Organic Frameworks. Angewandte Chemie International Edition. 2016;55:7188-93.
[61] Bae Y, Nishiyama N, Fukushima S, Koyama H, Yasuhiro M, Kataoka K. Preparation and biological characterization of polymeric micelle drug carriers with intracellular pH-triggered drug release property: tumor permeability, controlled subcellular drug distribution, and enhanced in vivo antitumor efficacy. Bioconjugate Chem. 2005;16:122-30.
[62] Hsu PP, Sabatini DM. Cancer cell metabolism: Warburg and beyond. Cell. 2008;134:703-7.
[63] Vaupel P, Kallinowski F, Okunieff P. Blood flow, oxygen and nutrient supply, and metabolic microenvironment of human tumors: a review. Cancer research. 1989;49:6449-65.
[64] Neri D, Supuran CT. Interfering with pH regulation in tumours as a therapeutic strategy. Nature reviews Drug discovery. 2011;10:767-77.

One-pot synthesis of pH-responsive charge-switchable PEGylated nanoscale coordination polymers for improved cancer therapy

Yu Yang, Ligeng Xu, Wenjun Zhu, Liangzhu Feng, Jingjing Liu, Qian Chen, Ziliang Dong, Jiayue Zhao, Zhuang Liu*, Meiwan Chen*

Key words: nanoscale coordination polymers (NCPs), one-pot synthesis, carrier-free drug delivery system, pH-responsive charge-switching, chemotherapy

TOC Figure:

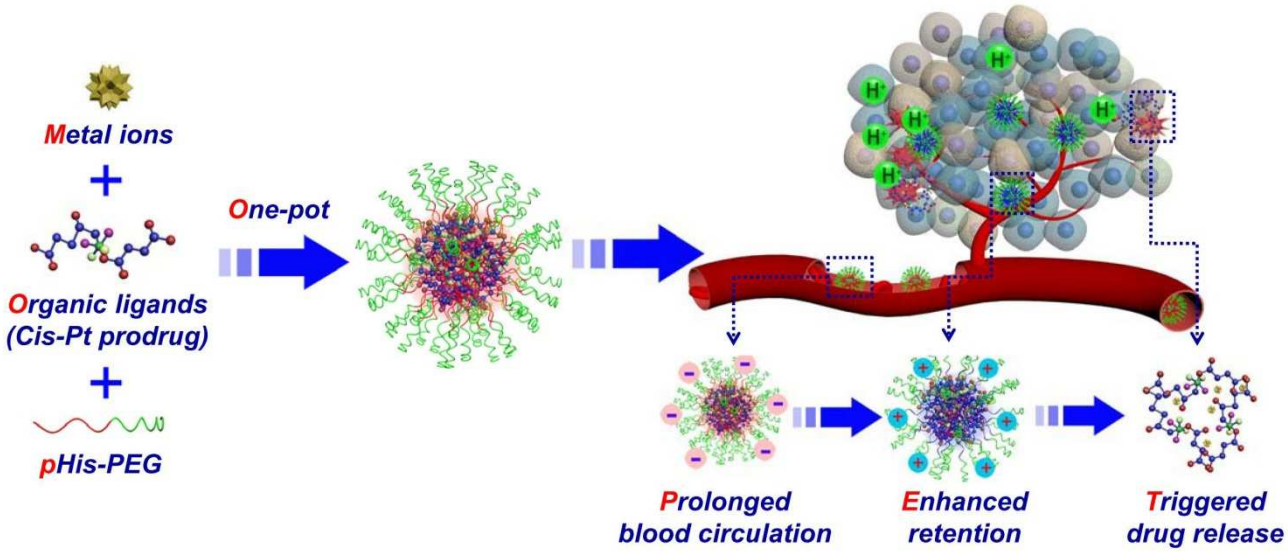

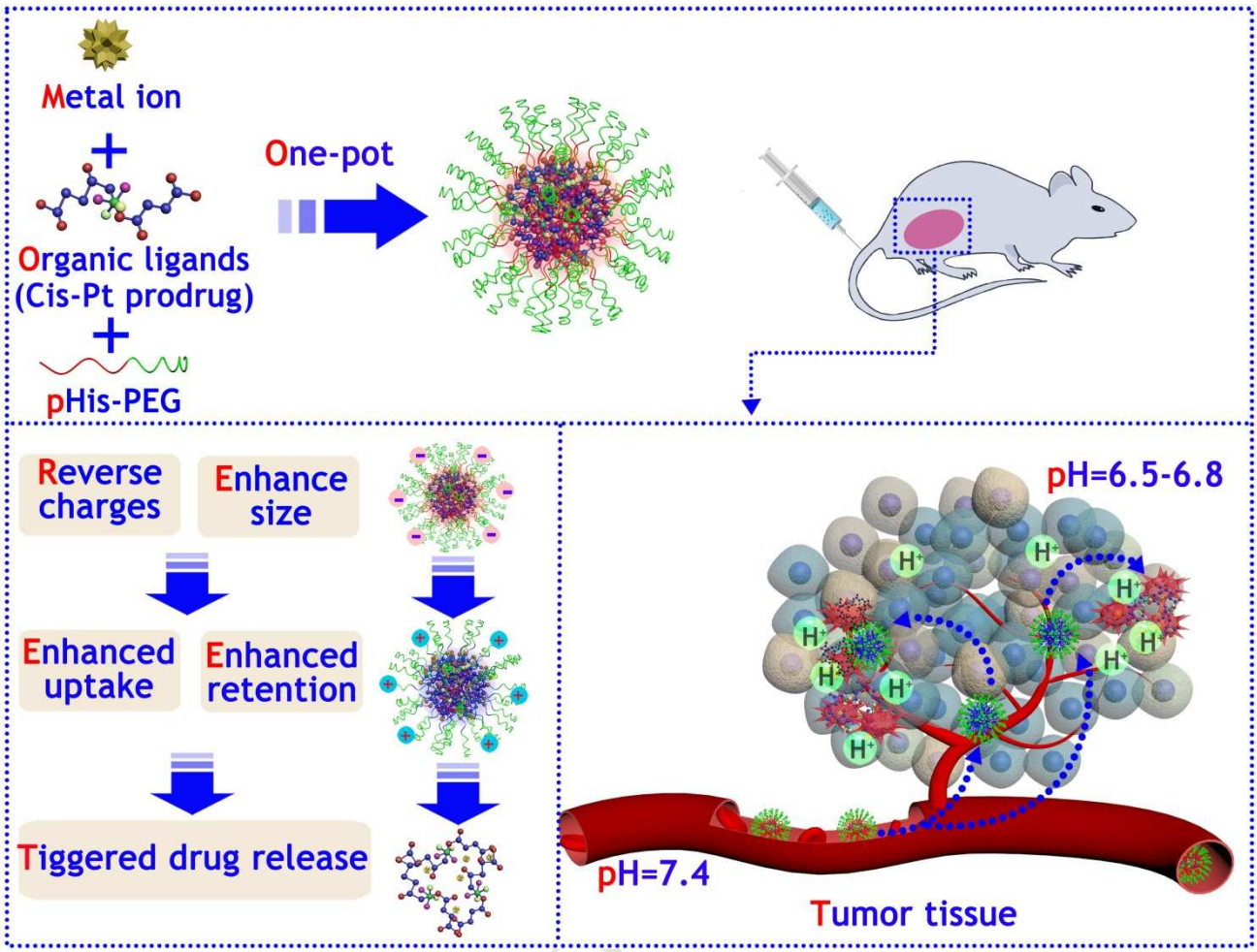

Scheme 1. A scheme illustrating the one-pot synthesis of PEGylated nanoscale coordination polymer (NCP-PEG) and their application for TME-responsive anticancer therapy.

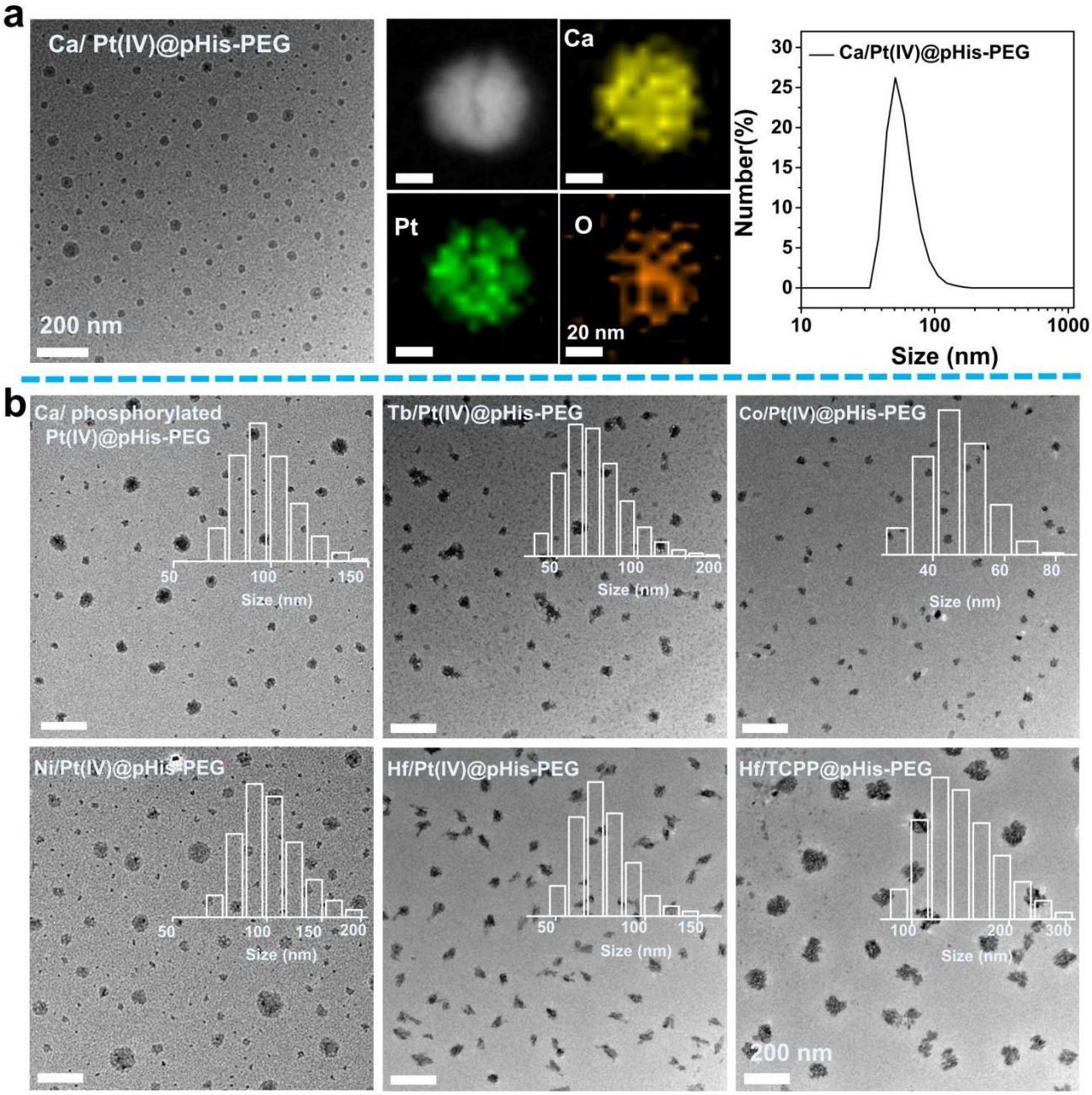

Figure 1. Characterization of NCP-PEG nanostructures. (a) A TEM image, STEM-EDS mapping and hydrodynamic diameters of Ca/Pt(IV)@pHis-PEG. (b) TEM images and DLS-measured diameters (inset figures) of Ca/ phosphorylated Pt(IV)@pHis-PEG, Co/Pt(IV)@pHis-PEG, Ni/Pt(IV)@pHis-PEG, Hf/Pt(IV)@pHis-PEG, Tb/Pt(IV)@pHis-PEG, and Hf/TCPP@pHis-PEG.

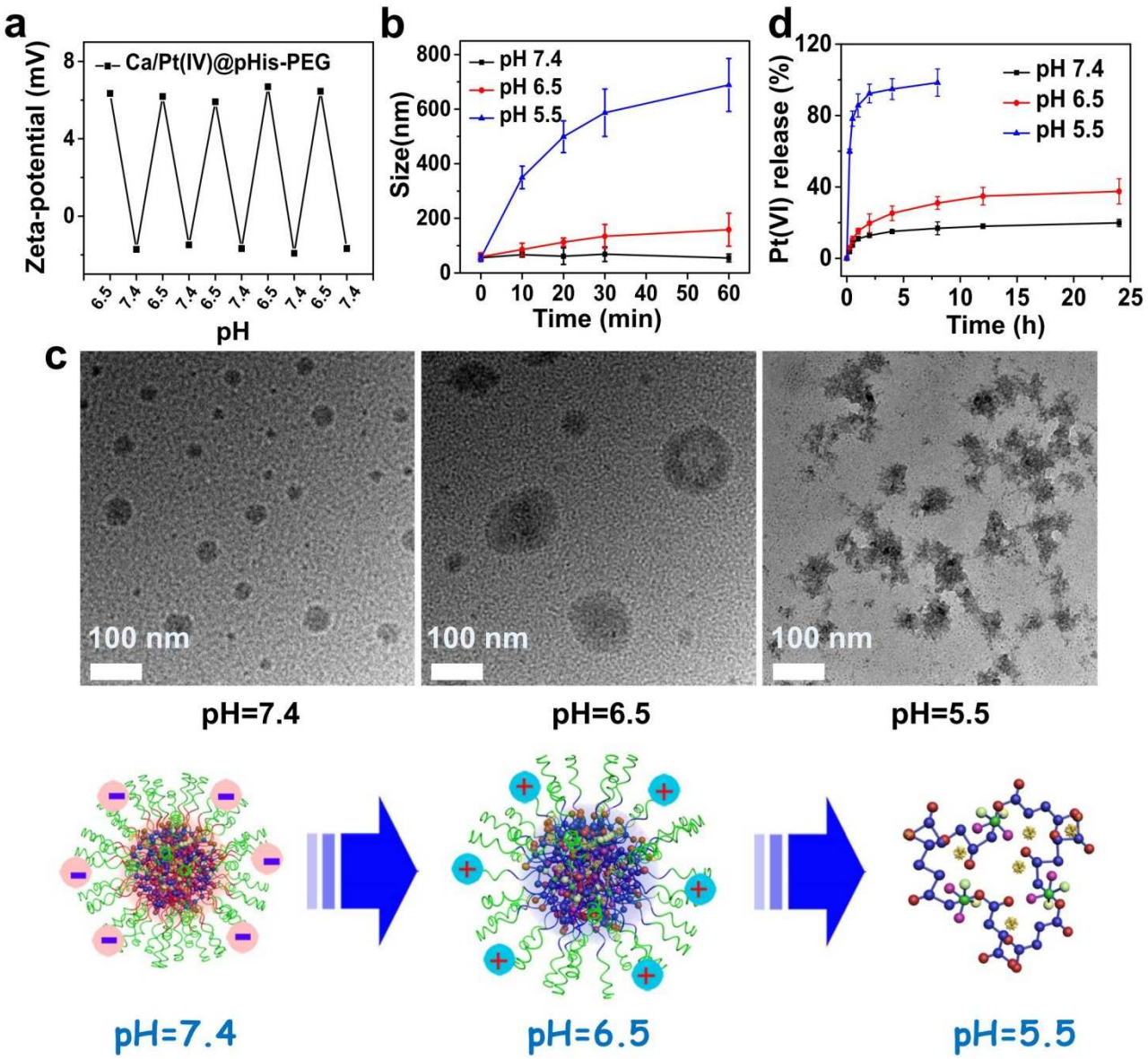

Figure 2. pH responsive properties of Ca/Pt(IV)@pHis-PEG. (a) Zeta potential changes of Ca/Pt(IV)@pHis-PEG after changing the solution pH between 6.5 and 7.4 for multiple cycles. (b) DLS-measured diameters of Ca/Pt(IV)@pHis-PEG incubated in PBS solutions with different pH values over time. (c) TEM images of Ca/Pt(IV)@pHis-PEG nanoparticles after incubation in PBS with different pH values for 60 min. (d) Cisplatin released from Ca/Pt(IV)@pHis-PEG over time in PBS at different pH values (7.4, 6.5 or 5.5). (e) The scheme illustrating pH-dependent morphology changes of Ca/Pt(IV)@pHis-PEG nanoparticles.

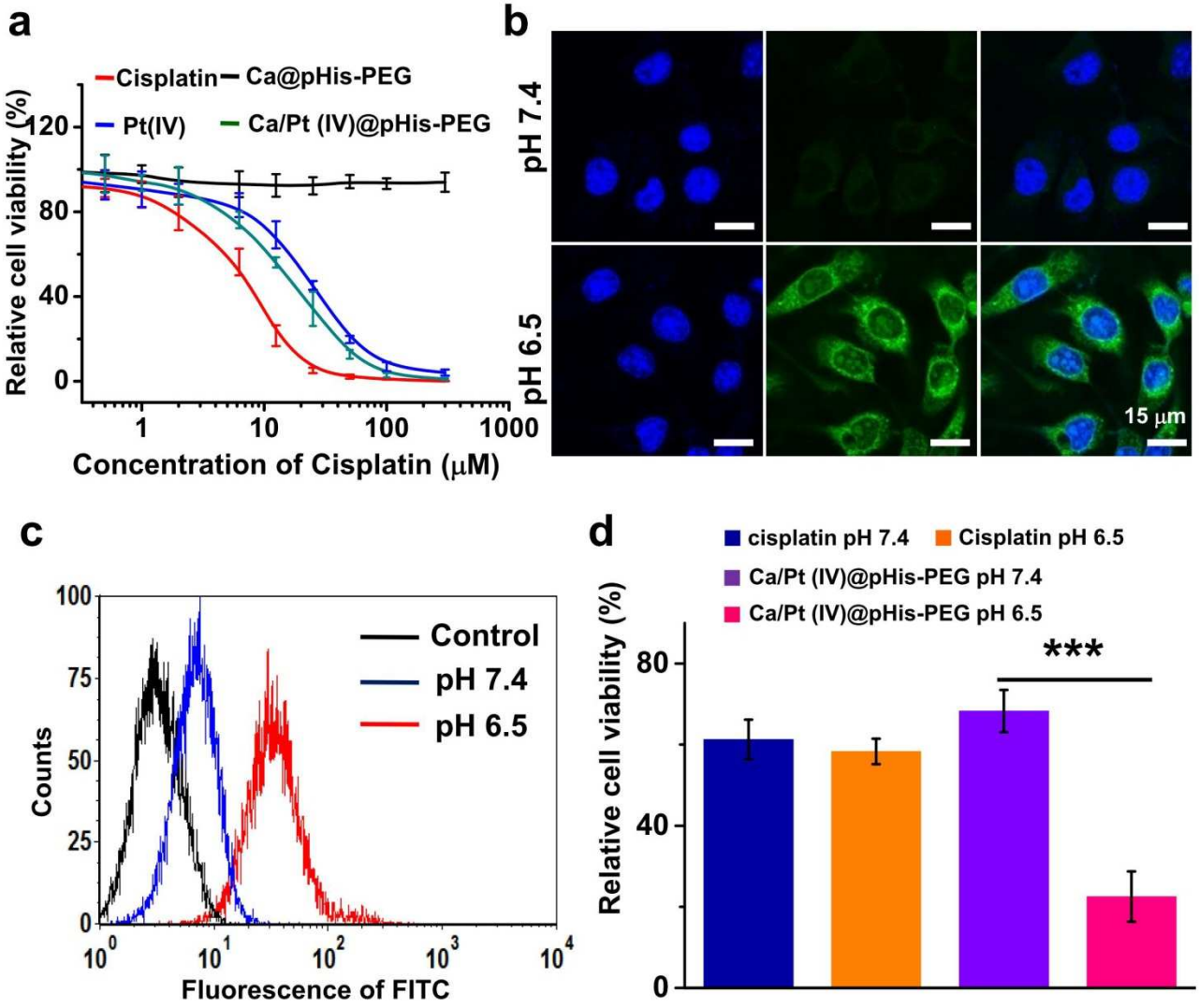

Figure 3. Intracellular internalization and in vitro cytotoxicity of Ca/Pt(IV)@pHis-PEG. (a) Relative viabilities of 4T1 cells after being treated with Ca@pHis-PEG, free cisplatin, free Pt(IV) prodrug and Ca/Pt(IV)@pHis-PEG at various concentrations for 48 h. (b) Confocal fluorescence images of 4T1 cells after being incubated with FITC-labeled Ca/Pt(IV)@pHis-PEG at pH 6.5 or 7.4 for 2 h. (c) Flow cytometry data of 4T1 cells after being incubated with FITC-labeled Ca/Pt(IV)@pHis-PEG at pH 6.5 or 7.4 for 2 h. (d) Relative viabilities of 4T1 cells after being treated by cisplatin and Ca/Pt(IV)@pHis-PEG at 25 μM of Pt under different pH values for 4 h. Ca/Pt(IV)@pHis-PEG showed enhanced cellular uptake and cytotoxicity under reduced pH. P values in (d) was calculated by Tukey's post-test (***$P < 0.001$, **$P < 0.01$ or *$P < 0.05$).

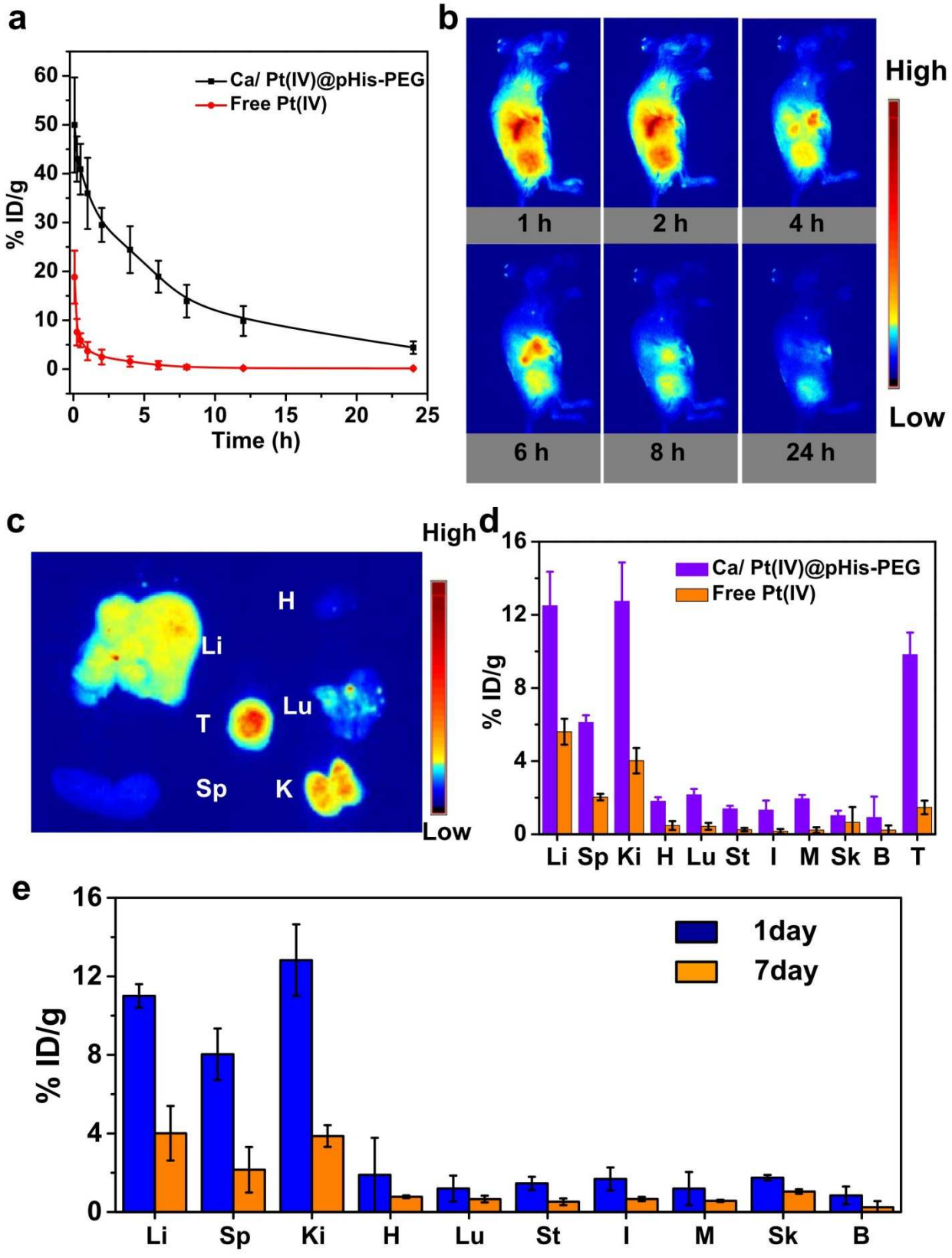

Figure 4. In vivo behaviors of Ca/Pt(IV)@pHis-PEG. (a) The blood circulation profiles of free Pt(IV) and Ca/Pt(IV)@pHis-PEG in 4T1 tumor mice over time. (b) Time-dependent in vivo fluorescence imaging of 4T1-tumor-bearing mice after i.v. injection of ICG-labeled Ca/Pt(IV)@pHis-PEG. (c) Ex vivo fluorescence images

of major organs taken at 24 h p.i. (d) Biodistribution profile of free Pt(IV) and Ca/Pt(IV)@pHis-PEG in 4T1 tumor-bearing mice at 24 h p.i. based on Pt levels determined by ICP-MS. Organ / tissue abbreviations: liver (Li), spleen (Sp), Kidneys (Ki), Heart (H), Lung (Lu), Stomach (St), Intestine (I), Muscle (M), Skin (Sk), Bone (B), and Tumor (T). (e) The biodistribution of Pt in healthy mice at 1 day and 7 days post i.v. injection of Ca/Pt(IV)@pHis-PEG.

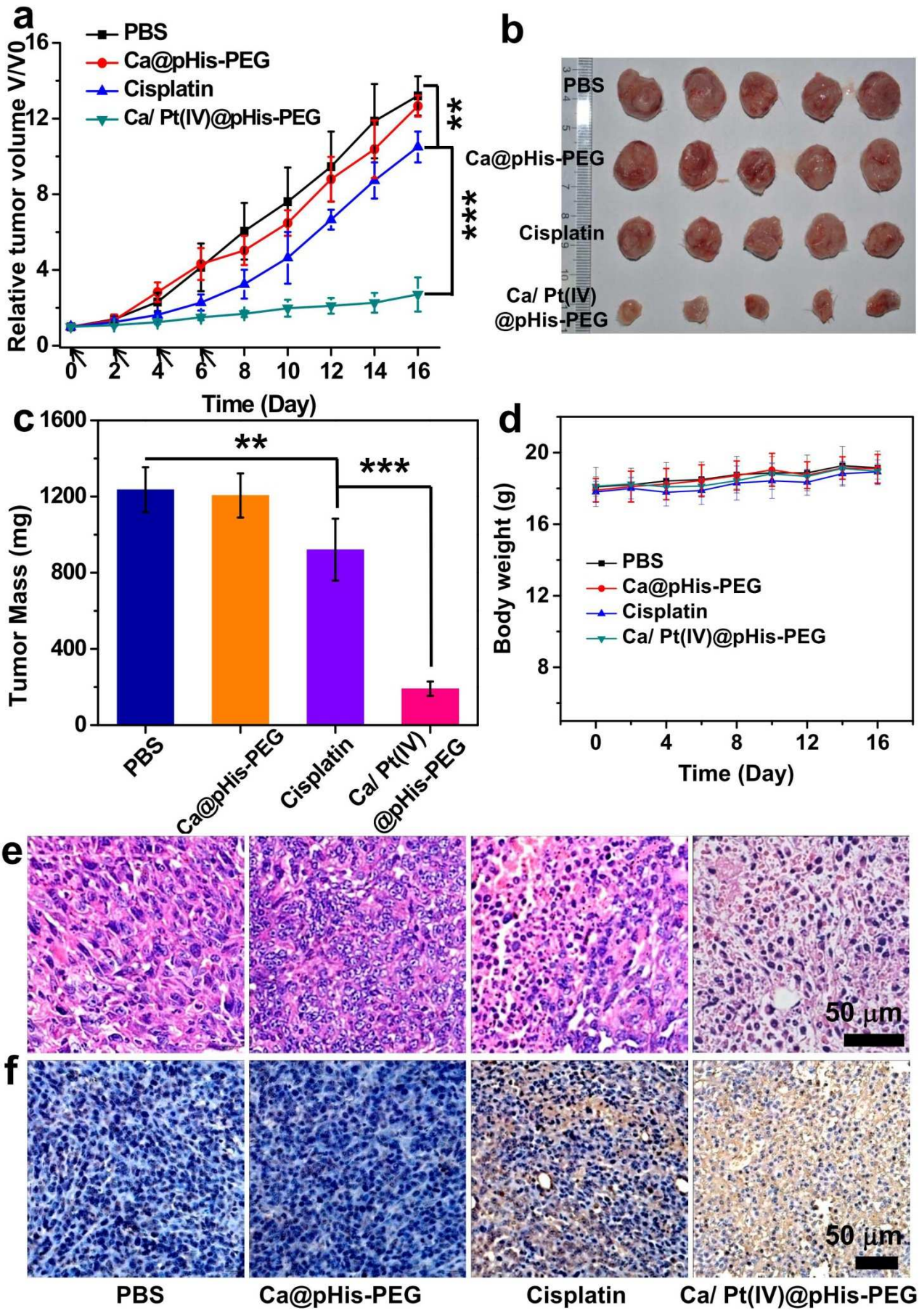
a
PBS
Ca@pHis-PEG
Cisplatin
Ca/ Pt(IV)@pHis-PEG
Relative tumor volume V/V0
Time (Day)
**
***
b
PBS
Ca@pHis-PEG
Cisplatin
Ca/ Pt(IV)
@pHis-PEG
c
Tumor Mass (mg)
**
***
PBS
Ca@pHis-PEG
Cisplatin
Ca/ Pt(IV)
@pHis-PEG
d
Body weight (g)
PBS
Ca@pHis-PEG
Cisplatin
Ca/ Pt(IV)@pHis-PEG
Time (Day)
e
50 μm
f
50 μm
PBS
Ca@pHis-PEG
Cisplatin
Ca/ Pt(IV)@pHis-PEG

Figure 5. In vivo anticancer therapy using Ca/Pt(IV)@pHis-PEG. (a) Tumor growth curves of 4T1-tumor-bearing mice after i.v. injection with PBS, free cisplatin, Ca@pHis-PEG, or Ca/Pt(IV)@pHis-PEG at indicated time points (cisplatin dose : 3 mg/kg for each injection). (b&c) Photographs (b) and average weights (c) of tumors collected from different groups 16 days after treatments were initiated. (d) Body weights of mice after various treatments indicated. (e&f) H&E (e) and TUNEL (f) stained tumor slices collected from different groups of mice at day 7 (one day after the last injection was given). P values in (a&c) were calculated by Tukey's post-test (***$P < 0.001$, **$P < 0.01$ or *$P < 0.05$).

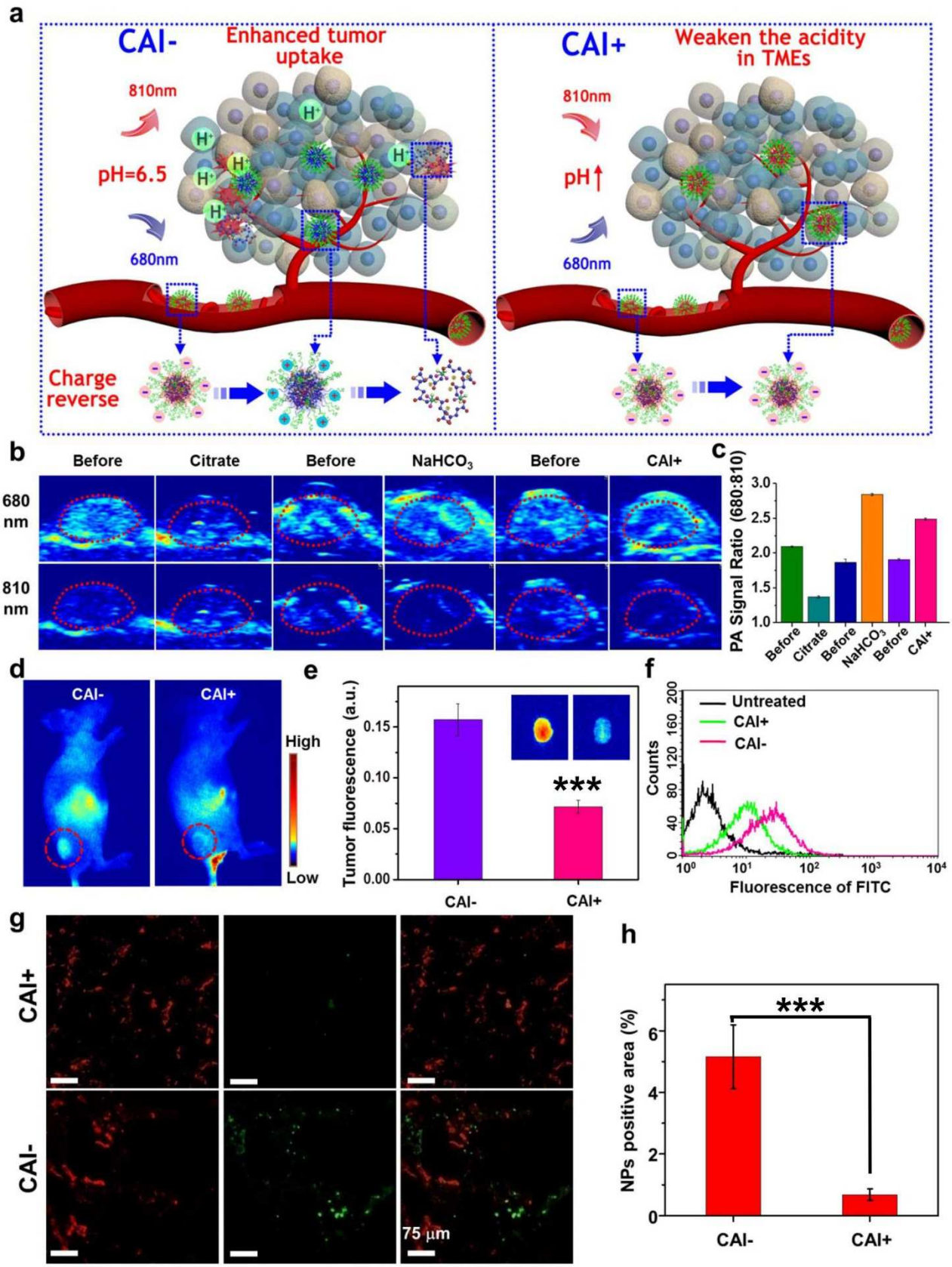

Figure 6. Mechanism study of pH-dependent cancer therapy with Ca/Pt(IV)@pHis-PEG NCPs. (a) A scheme illustrating the modulation of tumor pH using CAI to study the pH-dependent tumor accumulation / retention of

Ca/Pt(IV)@pHis-PEG. (b) PA images of tumors on mice before and after i.t. injection of citrate buffer (pH = 5.5), $NaHCO_3$ solution (pH = 8.4), or CIA. HAS-Croc as a PA imaging agent was i.v. injected into 4T1-tumor-bearing mice to in vivo pH detection under PA imaging. (c) The I_{680} /I_{810} PA signal intensity ratios, which are responsive to pH changes, in tumors based on PA imaging data in (b). Injection of CAI was able to induce significant increase in tumor pH. (d) In vivo fluorescence images of 4T1-tumor-bearing mice taken 24 h post injection of ICG-labeled Ca/Pt(IV)@pHis-PEG with and without their tumors treated with CAI. (e) Relative fluorescence intensities and ex vivo fluorescence images (inset) of the tumors with or without CAI treatment collected 24 h post injection of ICG-labeled Ca/Pt(IV)@pHis-PEG (f) Flow cytometry data of tumor cells collected from mice 24 h post injection of FITC-labeled Ca/Pt(IV)@pHis-PEG. (g) Confocal fluorescence images of tumor slices collected from mice 24 h post injection of FITC-labeled Ca/Pt(IV)@pHis-PEG. The green and red signals stand for FITC-labeled Ca/Pt(IV)@pHis-PEG and anti-CD31-stained tumor blood vessels, respectively. (h) Quantification of FITC signals based on confocal fluorescence images shown in (g). Owing to the increased tumor pH after CAI treatment, the tumor retention of Ca/Pt(IV)@pHis-PEG nanoparticles showed significant decrease. At the in vivo level, acidic pH is also favorable for enhanced cellular uptake of those nanoparticles. P values in (e&h) were calculated by Tukey's post-test (***$P < 0.001$, **$P < 0.01$ or *$P < 0.05$).